

A parametric study of Superconducting Solenoids

Giacomo Ragni,* Emanuele Terzini, and Emanuela Barzi†
Fermi National Accelerator Laboratory

(Dated: September 21, 2011)

An article usually includes an abstract, a concise summary of the work covered at length in the main body of the article.

The fully analytical model was implemented in MATHCAD code.

Usage: Secondary publications and information retrieval purposes.

PACS numbers: May be entered using the `\pacs{#1}` command.

Structure: You may use the `description` environment to structure your abstract; use the optional argument of the `\item` command to give the category of each item.

I. INTRODUCTION

One of the main challenges in high field solenoids is the large stress levels developed on the conductor due to Lorentz forces. To find parametric correlations useful in magnet design, analytical models can be used. An effective model is herein proposed to obtain the radial, azimuthal and axial stresses in a solenoid as a function of all the different parameters involved in this phenomenon.

II. ANALYTICAL MODEL

The model was divided into two different sections connected together: a magnetic model describing the magnetic field produced by the solenoid and the current density acceptable, a mechanical model describing the stresses in the coil and in the skin.

A. Magnetic model

The stresses on a solenoids are caused by the interaction between the magnetic field and the current, according to the Lorentz's force $\vec{F} = \int \vec{J} \times \vec{B}$, so first of all a magnetic model of the solenoid was created.

In a thick and finite-length solenoid [1] we can define the azimuthal component of vector potential as

$$A_\phi(r, z) = \frac{\mu_0}{4\pi} J(B) \int_{-\frac{L_c}{2}}^{\frac{L_c}{2}} \int_{R_1}^{R_2} \int_0^{2\pi} \frac{\cos(\theta)}{\sqrt{(z-l)^2 + r^2 + a^2 - 2ar\cos(\theta)}} d\theta da dl \quad (1)$$

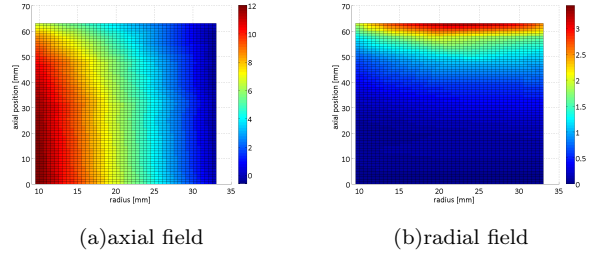


FIG. 1. Distribution of magnetic field in an half section of the coil

As a consequence of that the two components of the magnetic field (axial and radial) are respectively

$$B_z(r, z) = -\frac{1}{r} \frac{\partial [rA_\phi(r, z)]}{\partial r} \quad (2)$$

$$B_r(r, z) = -\frac{\partial A_\phi(r, z)}{\partial z} \quad (3)$$

Solving these two equations in an axial section of the coil the distributions shown in Figure 1 have been found.

The maximum self-field at the inner radius of the coil can be calculated more simply as [2]

$$B_0(\alpha, \beta) = R_1 \mu_0 J \beta \ln \left(\frac{\sqrt{\alpha^2 + \beta^2 + \alpha}}{\sqrt{1 + \beta^2 + 1}} \right) \quad (4)$$

where $\alpha = \frac{R_2}{R_1}$ and $\beta = \frac{L_c}{2} \frac{1}{R_1}$

The axial self-field was considered to have a linear distribution from $B_0(\alpha, \beta)$ at the inner radius to zero at the outer one. In case of an insert coil configuration the total field was calculated as the superposition of all fields [3]. The background field is constant in all the solenoid.

The radial self-field was considered to be constant along the radius and equal to $B_r(z) = B_r \left(\frac{R_1 + R_2}{2}, z \right)$, while the axial distribution was considered to be a parabola with its minimum in the mid plane, as shown in Figure2. The radial component of the background field was neglected.

* Also at Scuola Superiore Sant'Anna, Pisa

† barzi@fnal.gov

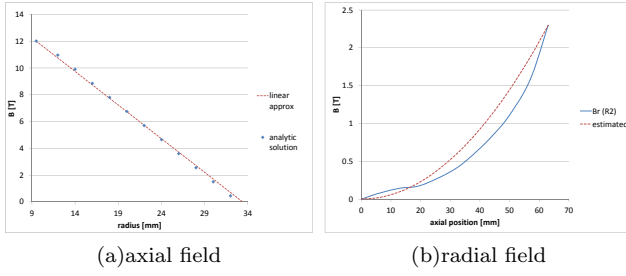


FIG. 2. Approximations of self-field

B. Mechanical model

The analytical mechanical model is based on a few assumptions, in order to be able to use simple equations and obtain results with little computational effort. The materials are supposed to be isotropic, linear, homogeneous and elastic, while actually the coil is realized with three different anisotropic materials (APPROFONDIRE O CITARE).

Only the mid plane stress distribution was considered because it was demonstrated and verified with FEM simulations in that it is the most loaded [4]. This is true under the hypothesis of "long" solenoid.

Firstly a classical approach have been used considering only the plane stress, then to determine axial stresses, the generalized plain strain approach was exploited. Finally the two results were coupled, because of the Poisson effects on deformations, obtaining the definitive stresses of the coil.

1. Planar stresses

Exploiting the axial symmetry of loads and geometry of the problem, it can be solved using Lamé's equation [5, 6], which is able to describe both the coil and the skin.

$$\frac{E}{1-\nu^2} \left(\frac{d^2 u}{dr^2} - \frac{1}{r} \frac{du}{dr} - \frac{u}{r^2} \right) + f = 0 \quad (5)$$

Depending on the load configuration, the expression of the term f has been considered to be

$$\begin{aligned} f &= J \cdot B(r) \text{ self field} \\ f &= J \cdot (B(r) + B_{out}) \text{ insert coil} \\ f &= 0 \text{ skin} \end{aligned}$$

The solution of the differential equation 5 both for coil and skin is

$$u(r) = C_1 r + \frac{C_2}{r} + u_0(r)$$

where $u_0(r)$ is a solution of the non homogeneous equation 5. In the generalized case of an insert coil,

$$u_0(r) = \frac{-(1-\nu^2) J(B_{tot})}{E} \left[\frac{B_0}{R_2 - R_1} \left(\frac{R_2 r^2}{3} - \frac{r^3}{8} \right) + B_{out} \frac{r^2}{3} \right] \quad (6)$$

The four coefficients can be determined imposing the boundary conditions on the free surface and at the interface between coil and skin.

$$\begin{aligned} \sigma_{rr,c}(R_1) &= 0 \\ \sigma_{rr,s}(R_2 + t) &= 0 \\ \sigma_{rr,c}(R_2) - \sigma_{rr,s}(R_2) &= 0 \\ u_{c2}(R_2) - u_{s2}(R_2) &= 0 \end{aligned} \quad (7)$$

Imposing a plane stress hypothesis, it is very simple to determine deformations, $\epsilon_{rr}(r) = \frac{du}{dr}$ and $\epsilon_{\theta\theta}(r) = \frac{u}{r}$ and stresses

$$\begin{aligned} \sigma_{rr}(r) &= \frac{E}{1-\nu^2} [\epsilon_{rr}(r) + \nu \epsilon_{\theta\theta}(r)] \\ \sigma_{\theta\theta}(r) &= \frac{E}{1-\nu^2} [\epsilon_{\theta\theta}(r) + \nu \epsilon_{rr}(r)] \end{aligned}$$

2. Axial forces

First of all the congruence of axial deformations was imposed. In particular, if we consider the mid-plane section of the coil, the axial stress is evaluated according to the generalized plain strain theory, which was considered the most adequate, considering that also during the magnetic modeling of the coil a similar hypothesis (long solenoid). As a consequence of that the axial stress is

$$\sigma_{zz}(r) = \nu [\sigma_{\theta\theta}(r) + \sigma_{rr}(r)] - \bar{\sigma}_{zz} \quad (8)$$

where $\bar{\sigma}_{zz} = 2 \int_{R_1}^{R_2} \nu [\sigma_{\theta\theta}(r) + \sigma_{rr}(r)] r dr$. Then the effect of the radial component of magnetic field was introduced, using a beam approach, so the stress can be evaluated as

$$\sigma_{zz_{magnetic}} = \frac{F_{axial}}{\pi (R_2^2 - R_1^2)} \quad (9)$$

where $F_{axial} = \int_0^{\frac{L_c}{2}} dF_{axial}$ determined taking into account the parabolic approximation and the Lorentz's force equation.

To increase the accuracy of the model, the effects of the axial stress were finally considered in the hoop and radial stresses taking into account the Poisson effects on deformations, superposing the effects and respecting all the boundary conditions. An estimation of the axial stress in the skin was obtained considering the friction between the outer surface of the coil and the inner surface of the skin.

3. Thermal effects

Thermal effects were considered only for planar stresses considering this law of deformation and imposing the boundary conditions of Equation 7

$$\begin{pmatrix} \sigma_{rr} \\ \sigma_{\theta\theta} \end{pmatrix} = \frac{E}{1-\nu^2} \begin{pmatrix} 1 & \nu \\ \nu & 1 \end{pmatrix} \begin{pmatrix} \epsilon_{rr} - \alpha\Delta T \\ \epsilon_{\theta\theta} - \alpha\Delta T \end{pmatrix} = \frac{E}{1-\nu^2} \begin{pmatrix} 1 & \nu \\ \nu & 1 \end{pmatrix} \begin{pmatrix} \frac{du}{dr} - \alpha\Delta T \\ \frac{u}{r} - \alpha\Delta T \end{pmatrix} \quad (10)$$

It is important to consider them because the coil and the skin have different coefficients of dilatation so, the changing in temperature between the assembly (25C) and the working (4.2K) creates stresses DA IMPEDITA DEFORMAZIONE. Generally the skin is more sensitive to temperature, so it is more compressed than the coil producing a decrease in the max coil hoop stress.

4. Assembly interference

Assembly interference between the coil and the skin was modeled defining a ΔU parameter which describes the intensity of this phenomenon. Actually, this effect can be obtained even applying a preload tension to the skin ropes, but the model is still good because, under our hypothesis, there's a linear dependence between ΔU and $T_{preload}$ and an analitic estimation have been developed in order to link the model with the manufacturing processes of coil:

$$F_{cable} \simeq \frac{L_c \int_{R_2+t}^{R_2+t} \sigma_{\theta\theta}(r) dr}{N_{AVVOLGIMENTI}}$$

The explicit relationship between ΔU and $T_{preload}$ depends on the geometry of the solenoid.

To obtain the analytic solution of the effect of the assembly interference, the principle of superposition of the effects have been exploited. First of all, the equation 5 has been resolved only for the skin simply imposing

$$\begin{aligned} f &= 0 \\ u(R_2) &= \Delta U \\ \sigma_{rr}(R_2 + t) &= 0 \end{aligned}$$

Then this solution was superposed to the standard one and all the stresses were calculated and the results, depending on the value of interference, are shown in Figure 3 where there is a comparison with the effect produced by thermal conditions.

5. Winding coil

The boundary conditions imposed to describe this effect are

$$\begin{aligned} u(R_1) &= W_{coil} \\ \sigma_{rr}(R_2) &= 0 \end{aligned}$$

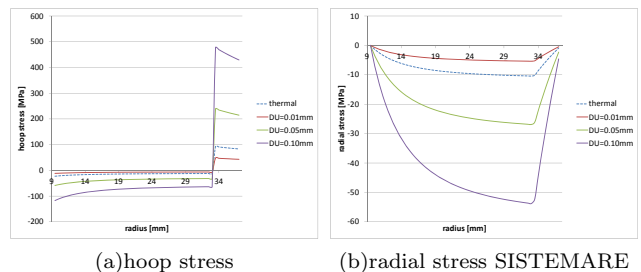


FIG. 3. Stresses due to assembly interference

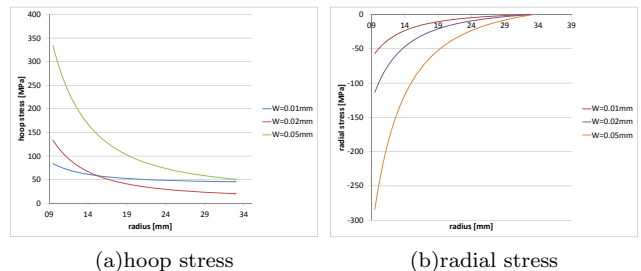


FIG. 4. Stresses due to winding coil

Solving the differential equation 5, the stresses in the coil due to different winding coil are shown in Figure 4

As shown in Figures 3 and 4, the assembly interference and the winding coil seem to have opposite effects on the stresses of the two components of the solenoid. The interference increases stresses on the skin, while the winding coil increases the coil stresses. Actually, both of them increase the stiffness of the structure reducing the maximum axial displacement of the coil, but they split the necessary stresses in different ways.

Starting from the knowledge of hoop stress in the coil it is possible to calculate an estimation of the necessary preload tension to be applied to the superconducting ropes to produce the desired effect exactly with the same approach used for the assembly interference.

C. Multiskin configuration

In order to obtain higher magnetic fields and to reduce the maximum stresses in the structure, a lot of new solutions of concentric coil have been developed.

In this geometry, described in the Appendix B the same Lamé's equation 5 can be used to describe the mechanical behavior of the structure, but new boundary conditions are needed, in order to determine 8 independent coefficients.

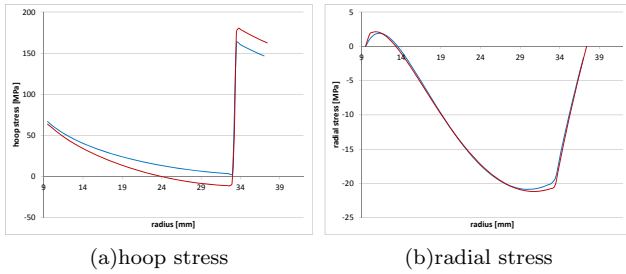


FIG. 5. Planar stresses in the self field solenoid

$$\begin{aligned}
 \sigma_{rr,c_1}(R_1) &= 0 \\
 \sigma_{rr,s_2}(R_2 + t_2) &= 0 \\
 \sigma_{rr,c_1}(R_m) - \sigma_{rr,s_1}(R_m) &= 0 \\
 \sigma_{rr,s_1}(R_m + t_1) - \sigma_{rr,c_2}(R_m + t_1) &= 0 \\
 \sigma_{rr,c_2}(R_2) - \sigma_{rr,s_2}(R_2) &= 0 \\
 u_{c_1}(R_m) - u_{s_1}(R_m) &= 0 \\
 u_{s_1}(R_m + t_1) - u_{c_2}(R_m + t_1) &= 0 \\
 u_{c_2}(R_2) - u_{s_2}(R_2) &= 0
 \end{aligned}$$

In this case the structure was supposed to be continuous with a perfect contact between the first skin and the second coil. This was done to reduce the stresses in the inner coil and to ease the manufacturing process and the design of the mechanical support of the solenoid.

Even in this case the hypothesis that the magnetic load acts only on the coil has been used. More over, the hypothesis of a linear behavior of the magnetic field was adopted neglecting the magnetic effect of a small steel skin between the two concentric coils.

The outer skin was considered to produce a background field for the inner one.

III. VALIDATION

To verify the accuracy of the analytical model proposed, the results obtained for two configurations described in Appendix B were compared with the results of a mesomechanic FEM model [7]. As shown in Figures 5 and 6 the distributions of plane stresses are perfectly coherent. In Figure 7 it is possible to appreciate that this new analytic model is able to foresee with good accuracy even the axial component of stress.

Finally in Table I there are the percentage differences between the two models, which are fully acceptable, considering the approximations and the uncertain knowledge of material properties. SISTEMARE

IV. RESULTS AND DISCUSSION

QUESTA DOVREBBE ESSERE LA PARTE SOSTANZIOSA

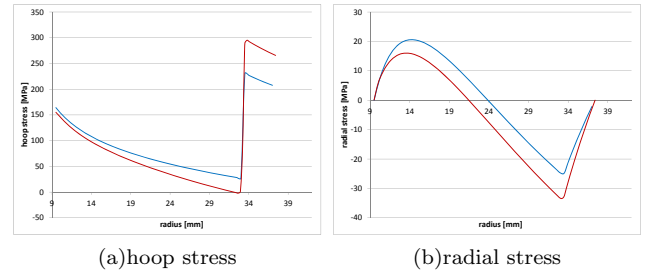


FIG. 6. Planar stresses in the insert coil solenoid

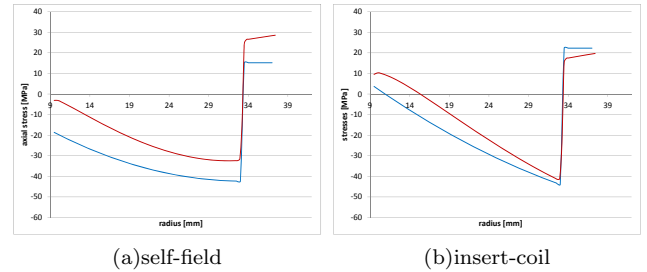


FIG. 7. Axial stresses

	self field	insert + 10T	insert + 20T
coil hoop	3.5%	3.7%	1.8%
coil radial	1.4%	5.9%	32%
coil axial	38%	13%	0.5%
skin hoop	2.8%	20%	26%
skin axial	28%	9.5%	35%

TABLE I. Difference between the models

Using the completely analytic model described in Section II it is possible to study the effects of all the parameters (geometric, physical and electromagnetic) on the mechanical behavior. In particular it is important to provide plots useful for future designs of superconducting solenoids in order to maximize the magnetic field and minimize stresses.

A. Sensitivity to physical constants

Because of the uncertain knowledge of material properties, it was important to study the sensitivity of the model to all the most important parameters

In particular it is very easy to realize that changing the ratio between the two Young modulus of the coil and the skin, it is possible to split up the stresses in the way we prefer.

In Figure 8 there are the plots of the relative variation of the hoop stress in the coil and in the skin depending on the variation of the following parameters:

- coil Young modulus ($E_c = 79.7GPa$)
- skin Young modulus ($E_s = 206GPa$)

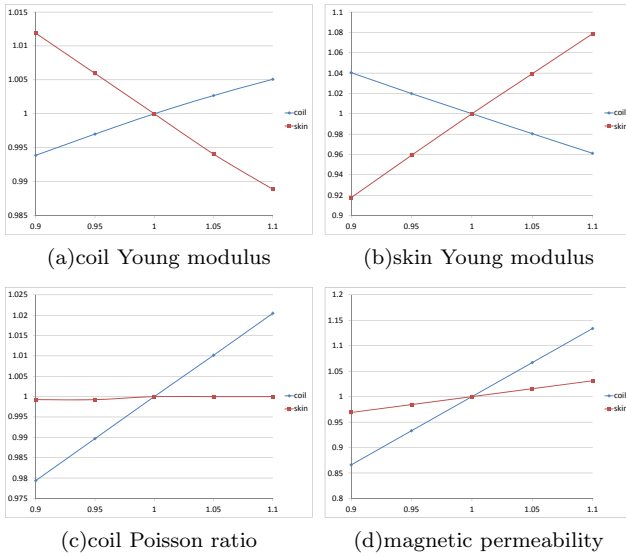


FIG. 8. Sensitivity of hoop stress to physical parameters

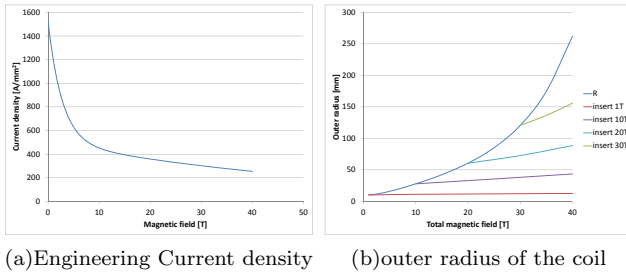


FIG. 9. Effects of the magnetic field

- coil Poisson ratio ($\nu_c = 0.3$)
- coil magnetic permeability ($\mu_0 = 79.7GPa$)

B. Effects of magnetic field

The maximum current density sustainable for an YBCO superconductor can be described as a function depending on the magnetic field as described in the Appendix IV B. APPROFONDIRE

As shown in Figure 9 an higher total magnetic field makes the solenoid wider and the maximum current density acceptable lower. Actually, the first effect depends also on the type of this magnetic field because, as shown in Equation 4 the magnetic field produced by a solenoid is directly proportional to the current density inside the coil, which depends on the total magnetic field (self-field and background).

One of the most important results obtained by this parametric study are the laws of maximum stresses depending on the total magnetic field, whose plots are shown in Figure 10. It has been demonstrated that the hoop stress depends not only on the value of the total

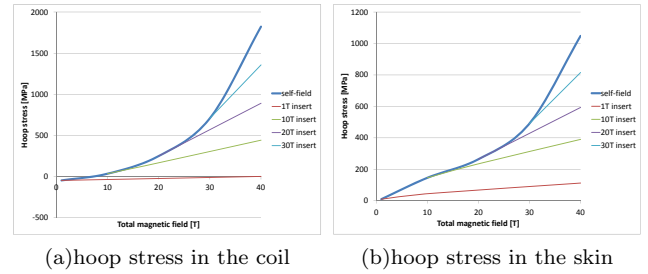


FIG. 10. Hoop stresses in solenoids at constant magnetic field

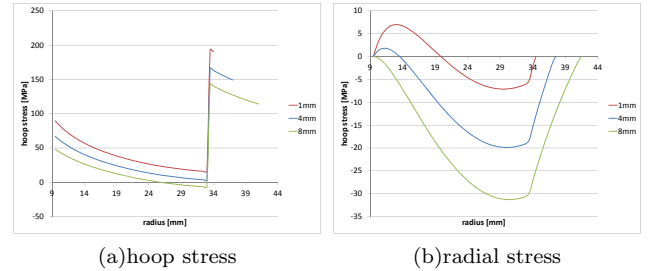


FIG. 11. Effects of the skin thickness

magnetic field, but also on its kind. A smaller solenoid in a huge background field is less loaded than a huge solenoid producing the same self field.

C. Effects of geometric parameters

Usually the dimensions of the inner radius and the axial length of the solenoid are imposed, while the outer radius is determined by the self-field desired. In order to manage the stress distribution in the solenoid it is possible to change the skin thickness obtaining the effects shown in Figure 11.

D. Effects of winding coil and assembly interference

Considering the geometry and the loading configuration described in the Appendix B, it is possible to study the effect of the manufacturing processes of the solenoid on its mechanical behavior. In fact, as shown in Figure 12 and in Figure 13, the preload on the ropes produce considerable effects on the stresses.

The two processes seems to produce exactly two opposite effects:

- the assembly interference decreases the coil hoop stress while it increases the skin hoop stress and the maximum radial stress
- the winding coil decreases the skin hoop stress and the maximum radial stress while it increases the coil hoop stress.

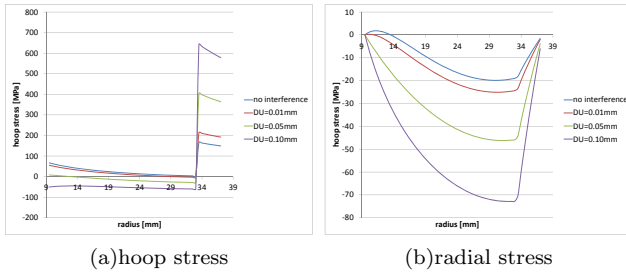


FIG. 12. Effects of interference on stresses at the working condition

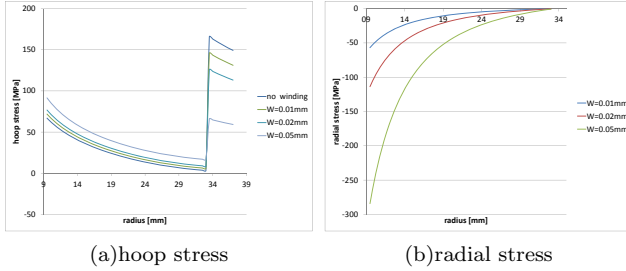


FIG. 13. Effects of winding coil on stresses at the working condition

Actually it is important to emphasize that these effects depend on the particular geometry and, more in detail, on the thickness of the steel skin as can be understood looking at Figure 11.

1. Combinations of the effects

The task of minimizing stresses in the coil and in the skin can be reached considering both the effects of winding coil and assembly interference combined together and superposing the solutions obtained from Equation 5. In Figure 14, it is possible to see that there is a minimum of the hoop stress intensity in the coil. This minimum is due to the fact that we are considering the absolute value of the hoop stress and, after a determined value of interference, the compression stress becomes more critical than the tension one. So it is possible to determine a couple of values for the interference and the winding coil to have a fixed value of stress in the coil.

E. Multiskin configuration

In this configuration (see Appendix B 2) there are more geometrical parameters to set to design the solenoid, so it is possible to optimize better the combination of the effects in order to minimize stresses or to maximize the magnetic field.

First of all it is important to compare the distributions of stresses between a continued single coil solenoid and

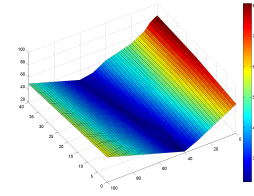


FIG. 14. Hoop stress in the coil due to interference and winding

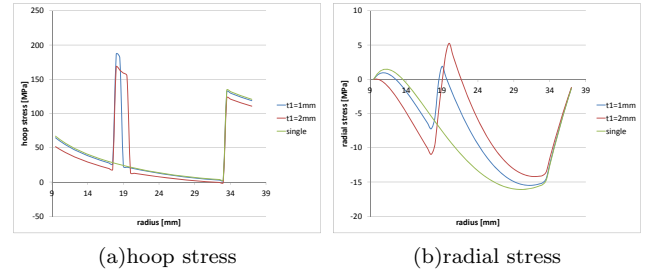


FIG. 15. Stress comparison

a multiskin configuration with different thickness of the intermediate skin, as shown in Figure 15.

The self field of the outer coil was considered to be a constant background field.

To modify the peak stresses it can be simple and useful to modify the material of the first skin, so a sensitivity analysis was performed and the results are shown in Figure 16.

Using a less stiff material, it is possible to decrease the stress on the skin without increasing it too much in the coil and allowing an higher magnetic field.

To maximize the coil efficiency it was assumed that each coil section operates at its own minimum critical current density [3]. The inner coil has a critical current density lower than the outer one, so its outer radius can be varied to maximize the self-field of the double-coil. In Figure 17 is shown the total magnetic fields depending on R_m and on the thickness of the first skin. It is very easy to understand that it is possible to obtain an higher magnetic field with the same radial bulk.

Exploiting this important result, in Figure 18 it is

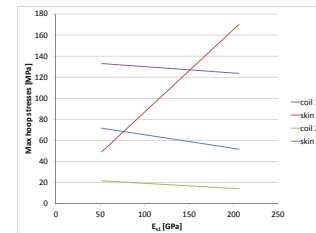


FIG. 16. Maximum hoop stresses depending on the Young modulus of the inner skin

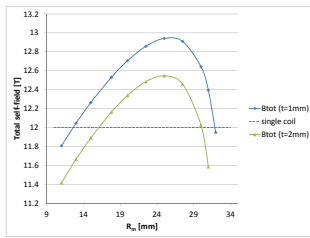
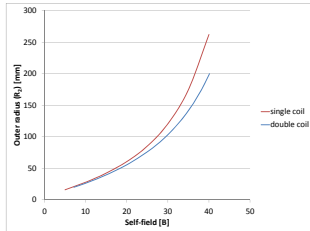
FIG. 17. Total self-field depending on R_m 

FIG. 18. Outer radius

shown the relationship between the total magnetic self-field on a single coil configuration and a double-coil configuration, where R_m was imposed to be the arithmetic average between R_1 and R_2 . Just to have an idea of the possible material saving, for a $40T$ field the two outer radius are respectively $262mm$ and $198mm$ with a difference in volume of the 43%.

V. CASE STUDIES

This analytical model has been used to describe the magnetic behavior of three real configurations of solenoids used in the most important laboratories of the country:

- National High Magnetic Field Laboratory (NHMFL)
- Francis Bitter Magnet Laboratory at Massachusetts Institute of Technology (FBML-MIT)
- Brookhaven National Laboratory (BNL)

All the configurations studied were realized and tested taking into account almost only magnetic and electric parameters, but now it is possible even to consider analytically the mechanical behaviors and optimize the configurations.

CI VORREBBERO DEGLI ARTICOLI DA CITARE E DELLE INTRODUZIONI AI SINGOLI COIL

A. National High Magnetic Field Laboratory

The coil Y10-3 was considered. The geometry is described in Table II.

$$\begin{aligned} R_1 & 7.15mm \\ R_2 & 19mm \\ L_c & 100mm \end{aligned}$$

TABLE II. NHMFL coil geometry

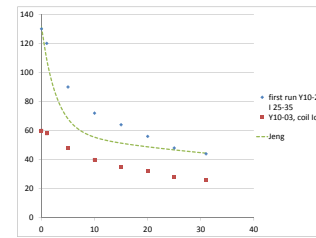


FIG. 19. Critical current in NHMFL coil

Considering a tape width of $4.00mm$ and a thickness of $195.00\mu m$, the Engineering Current Density was calculated using our model and in Figure 19 is shown the comparison between the experimental data obtained at NHMFL and our analytic distribution.

The configuration studied to calculate the mechanical stresses is the same used at NHMFL to determine the critical current, an insert coil with a background field of $31T$. The stresses obtained are shown in Figure 20.

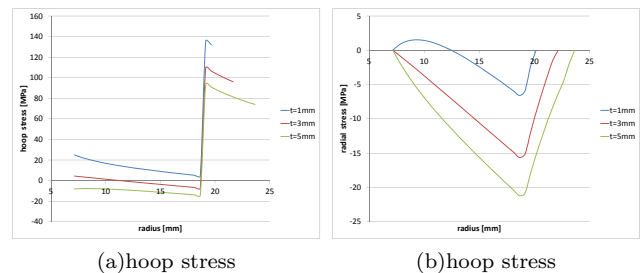
COMMENTI

B. Francis Bitter Magnet Laboratory - Massachusetts Institute of Technologies

This configuration is a multiskin with two coils both realized in High Temperature Superconductors: the inner one is realized in YBCO while the outer is in Bi2223. The geometry and the materials properties are all listed in Tables III and IV.

Considering the self-field loading configuration with the magnetic fields of Tables III and IV the stresses obtained are shown in Figure 21. Three different skin configurations were considered in order to have a better idea of its influence on the mechanical behavior of the structure.

The skin is very useful to reduce the hoop stress in the coil and, optimizing its thickness, it is even possible to control the max radial stress in the coil in order to avoid



(a) hoop stress

(b) hoop stress

FIG. 20. Stress in NHMFL coil

R_1	74mm
R_2	142.3mm
L_c	462.2mm
E_{YBCO}	79.7GPa
J	19.94 $\frac{A}{mm^2}$
B_0	8.33T

TABLE III. MIT insert 1

R_1	158.3mm
R_2	221.3mm
L_c	518.2mm
E_{Bi2223}	106GPa
J	15.50 $\frac{A}{mm^2}$
B_0	5.76T

TABLE IV. MIT insert 2

sliding among ropes. Both the configurations with an air interface and without have been considered emphasizing the different effects they produce in the distribution of stresses.

Actually, at Francis Bitter Magnet Laboratory the task is realizing lots of insert coils all concentric, so to have a better idea of the real stresses of the most loaded coils (the inner ones) the same geometry was loaded with a background magnetic field of 30T and the results are shown in Figure 22.

C. Brookhaven National Laboratory

This last configuration was taken by the Brookhaven National Laboratory [11] among the geometries developed for muon colliders. Even in this case, the geometry is made of two concentric solenoids whose characteristics are described in Tables V and VI

Figure 23 shows the stresses of the two coils with no preload. We verified that, applying a 1 GPa inner-magnet banding pre-stress the resulting stresses agree with those obtained at Brookhaven National Laboratory with an FEM simulation as shown in Table VII

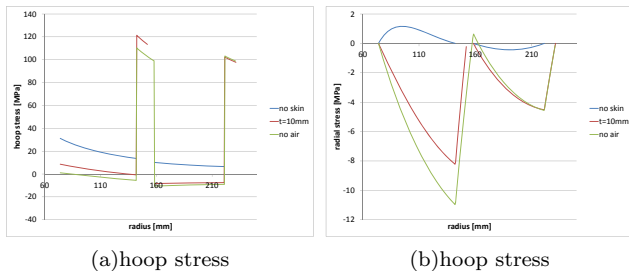


FIG. 21. Stress in FBML-MIT coils

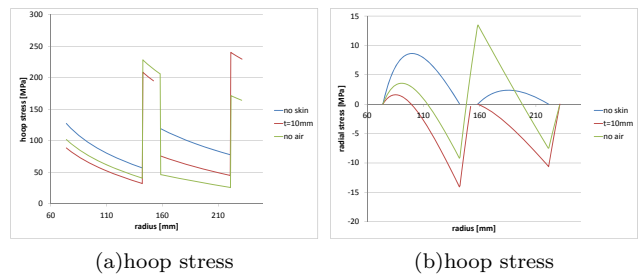


FIG. 22. Stress in FBML-MIT coils with 30T background field

R_1	25mm
R_2	90mm
L_c	64mm
B_0	10T

TABLE V. BNL insert 1

VI. CONCLUSION

As shown in all these parametric studies, the design of superconducting solenoid is influenced by a number of parameters. The development of a fully analytic model able to describe all these complex phenomena is important to have an idea of the effects of the any of them on the stresses or on the magnetic field. The plots of Section IV will be used by solenoids designer to better understand these effect and to obtain optimized configurations depending on their tasks. COSA CI SI SCRIVE???

Appendix A: Material properties

The physical properties of the materials composing the coil and the steel of the skin are listed in Table VIII [8].

1. Averaged Young Modulus

The superconductor rope is composed of three different materials as shown in Figure 24. To calculate the Young modulus for the analytical model the areas of the different materials were considered and an averaged modulus was chosen, using the data in VIII. As a consequence of

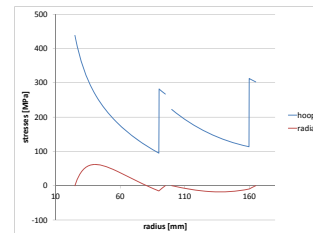


FIG. 23. Stresses without pre-stress

R_1	100mm
R_2	160mm
L_c	128mm
B_0	12T

TABLE VI. BNL insert 2

<i>Fermilab Brookhaven</i>	
max coil hoop stress	327MPa 260MPa
max skin hoop stress	1.2GPa 1.1GPa

TABLE VII. Self-field configurations

Material	E (GPa)	ν	$\alpha_{???}$ (K^{-1})
YBCO	110	0.3	$8 \cdot 10^{-6}$
Kapton	5.5	0.3	
Epoxy	4.5	0.3	
Steel	206	0.3	$10 \cdot 10^{-6}$

TABLE VIII. Materials' properties

that in all the results shown in this article the coil was supposed to be homogeneous with a Young modulus of

$$E_{coil} = 79.7GPa$$

Of course this is only an approximation, but it has been verified that the results perfectly agree with a FEM mechanical model taking into account the exact composition of the coil.

2. Engineering Current Density

The Engineering Current Density, shown in Figure 9, represents the limit for the current density in the coil that can't be exceeded [9]. It has been defined as a function of the total magnetic field in the solenoid. It has been determined fitting experimental results and its analytical expression is

$$J_c = c_1 e^{-c_2 B} + c_3 e^{-c_4 B} \quad (A1)$$

where the coefficients at 95% confidence level have the following values:

$$\begin{aligned} c_1 &= 1018 \\ c_2 &= 0.3606 \\ c_3 &= 503.3 \\ c_4 &= 0.01702 \end{aligned}$$

Appendix B: Geometric configuration

In this section there are all the data of the geometries of the solenoids used to perform all the parametric studies on the two different configurations: single and double coil.



FIG. 24. Geometry of the elementary cell of the coil

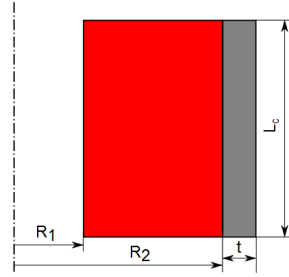


FIG. 25. Geometry of the solenoid

R_1	9.5mm
R_2	33.4mm
L_c	126mm
t	4mm
J_{eng}	$4.238 \cdot 10^8 \frac{A}{m^2}$
B_0	12T
$B_r(\frac{L_c}{2})$	3.435T

TABLE IX. Definition of the standard solenoid

R_1	9.5mm
R_2	33.4mm
R_m	17.8mm
L_c	126mm
t_1	1mm
t_2	4mm
$J_{1,eng}$	$???? \cdot 10^8 \frac{A}{m^2}$
$J_{1,eng}$	$???? \cdot 10^8 \frac{A}{m^2}$
B_0	??T

TABLE X. Definition of the standard solenoid for double coil configuration

1. Single coil

The geometry considered in this work is shown in figure 25. To validate the analytic model and to run all the parametric studies a standard solenoid was defined [4] as described in Table IX

2. Double coil

Here in Figure 26 the geometry of the double coil configuration is described while all the significant dimensions of the standard solenoid are in Table X.

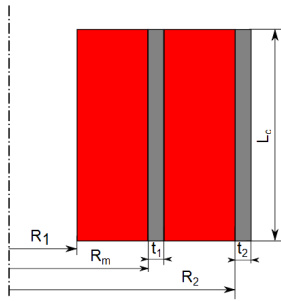


FIG. 26. Geometry of the solenoid

This multiskin configuration may also be studied introducing an air gap between the first skin and the second coil in order to reduce the maximum stresses and have a better cooling, but generating some manufacturing problems.

-
- [1] G. Brown, L. Flax, and E. Itean, *Axial and radial magnetic fields of thick finite length solenoids*, Tech. Rep. TN D-1993 (NASA, 1963).
 - [2] M. Wilson, *Superconducting Magnets* (Oxford Science Publications, 1983).
 - [3] V. Kashikhin, E. Barzi, V. Kashikin, M. Lamm, Y. Sadovskiy, and A. Zlobin, IGNOTO (IGNOTO).
 - [4] G. Ragni and E. Barzi, *A parametric study of Superconducting Solenoids*, Tech. Rep. TO BE DEFINED (FERMILAB, 2011).
 - [5] M. Beghini, *Dispense di Tecnica delle Costruzioni Meccaniche* (SEU Unipi, 2009).
 - [6] S. Timoshenko, *Strength of materials* (Princeton, 1956).
 - [7] A. Bartalesi, *Design of High Field Solenoids made of High Temperature Superconductors*, MASTERS 04 (FERMILAB, 2009).
 - [8] J. Ekin, *Experimental techniques for low-temperature measurements* (Oxford University Press, 2006).
 - [9] E. Terzini and E. Barzi, *Analytical Study of Stress State in HTS Solenoids*, Tech. Rep. TM-2448-TD (FERMILAB, 2009).
 - [10] R. Juvinall and K. Marshek, *Fondamenti della progettazione dei componenti delle macchine* (ETS, 1993).
 - [11] R. Gupta and al., PAC (2011).